Electronic Supplementary Material (ESI) for RSC Advances.

In situ high-valued transformation of nonmetals in waste printed circuit boards into supercapacitor electrode with excellent performance

Zhen Xi [a], *Ruitong Gao* [a]*, *Zhaojun Chen* [a]*, *Hui Du* [a], *Zhenming Xu* [b]

[a] College of Chemistry and Chemical Engineering, Institute for Sustainable Energy and Resources, Qingdao University, Qingdao, 308 Ningxia Road, Qingdao 266071, P.R. China

[b] School of Environmental Science and Engineering, Shanghai Jiao Tong University, 800 Dongchuan Road, Shanghai 200240, P.R. China

Corresponding author: Ruitong Gao; Zhaojun Chen

E-mail: gaoruitong@qdu.edu.cn; chenzj_upc@126.com

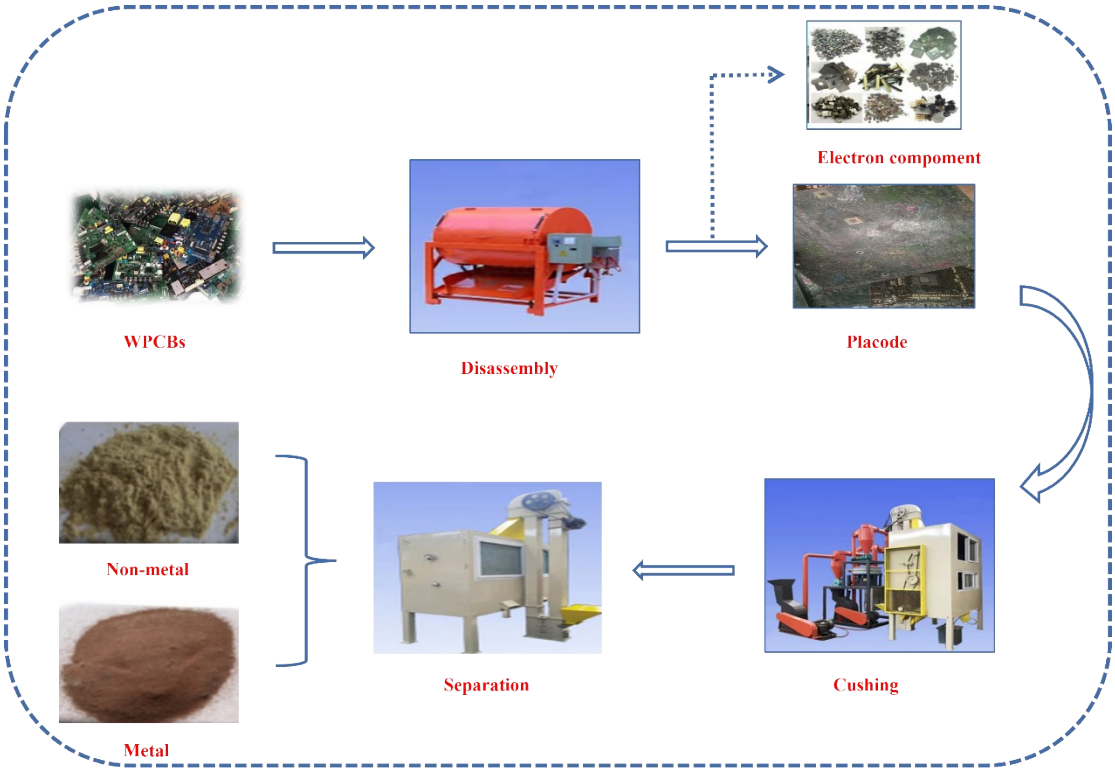

Fig. S1. Pretreatment process of WPCBs.

Text 1 measurement method for NMFs composition before and after acid leaching pretreatment

The compositions of NMFs before and after acid leaching pretreatment was determined by X-ray Fluorescence (XRF, Thermo Scientific, Waltham, MA). Before analysis, all samples were homogenized to powder form. Total duration of measurement was 300 s. The detection limits of main elements were -0.0025 wt % and trace elements were3-600ppm. All samples were analyzed in three repeats (results of analyses were arithmetic mean, the relative standard deviation was <5%).

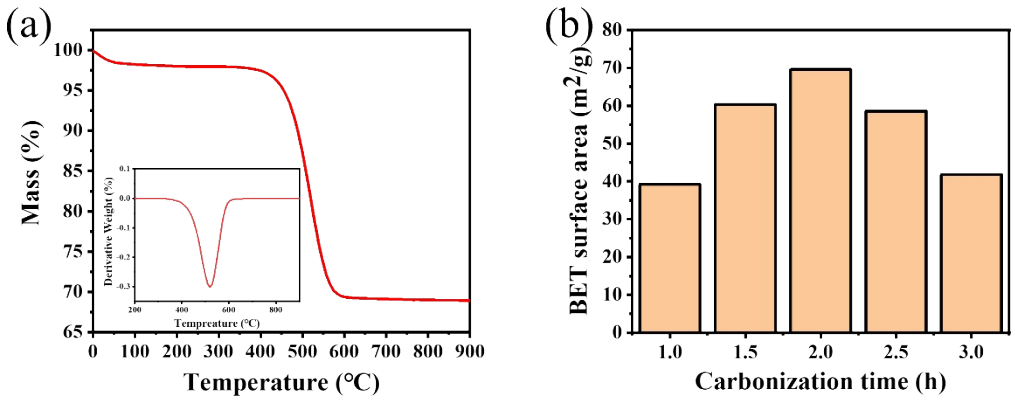

Fig. S2. (a) TG and DTG curve of NMFs; (b) Effect of carbonization time on specific surface area of pyrolytic residues.

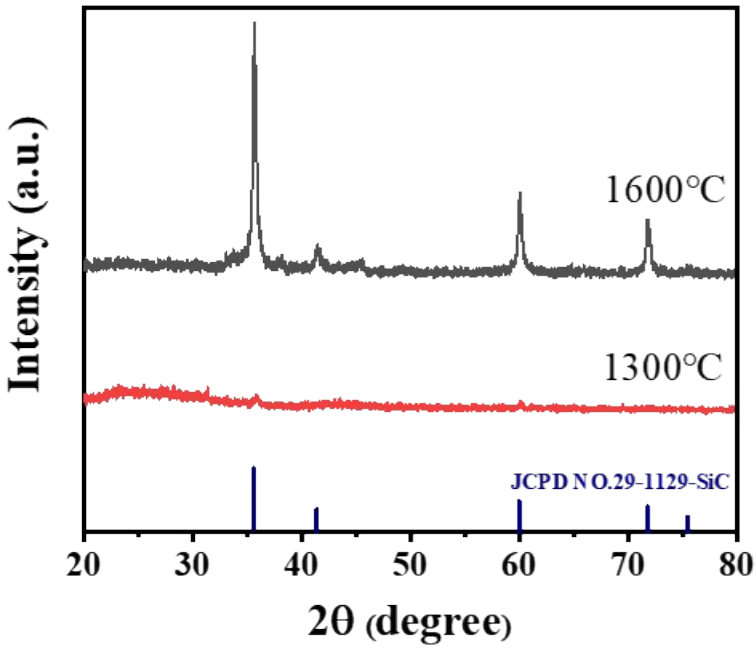

Fig. S3. XRD spectra of electrode material at different temperatures.

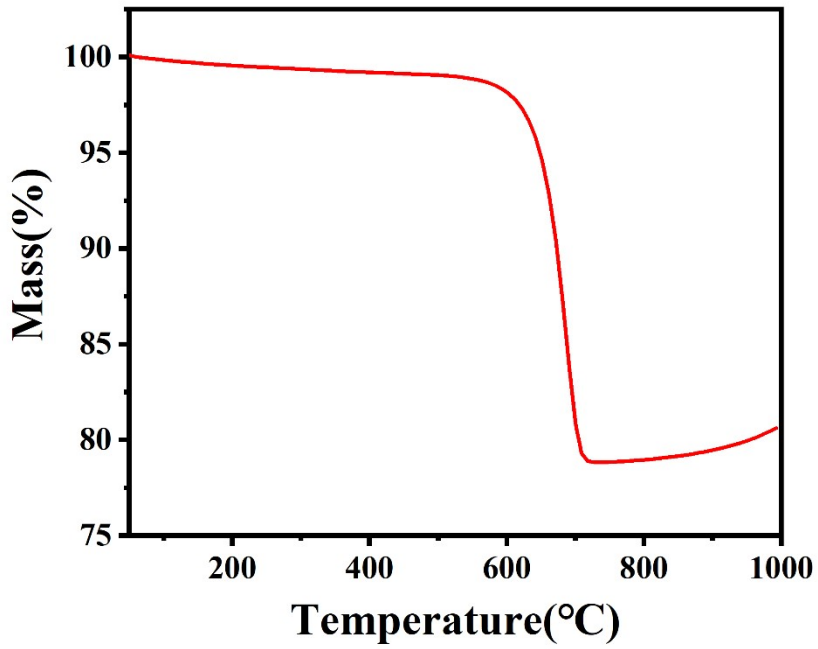

Fig. S4. TG curve of electrode material.

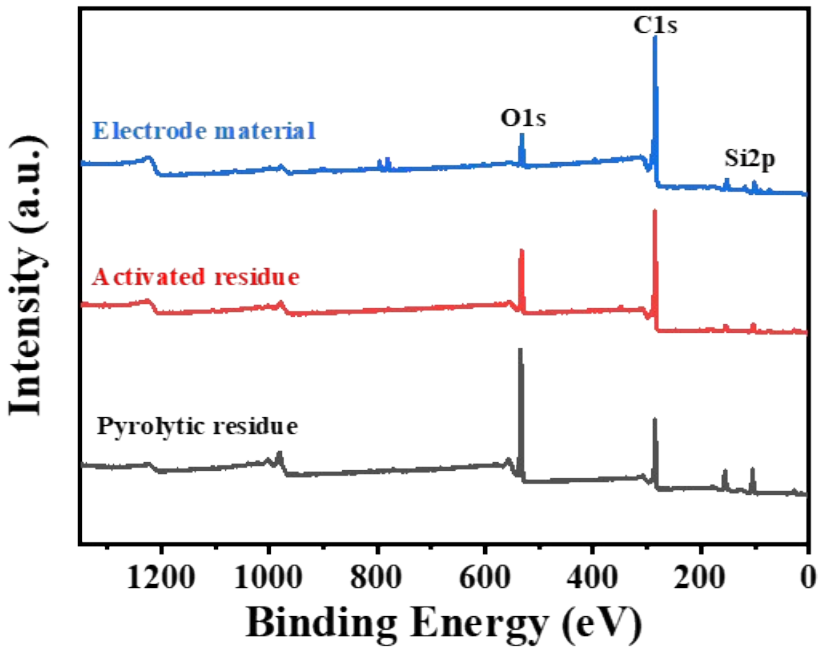

Fig. S5. XPS spectra of pyrolytic residues, activated residues and electrode material.

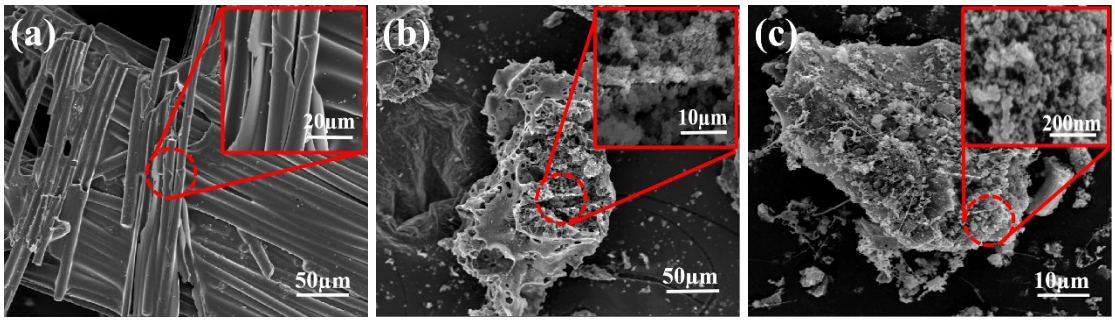

Fig. S6. SEM images of (a) pyrolytic residues, (b) activated residues, (c) electrode material.

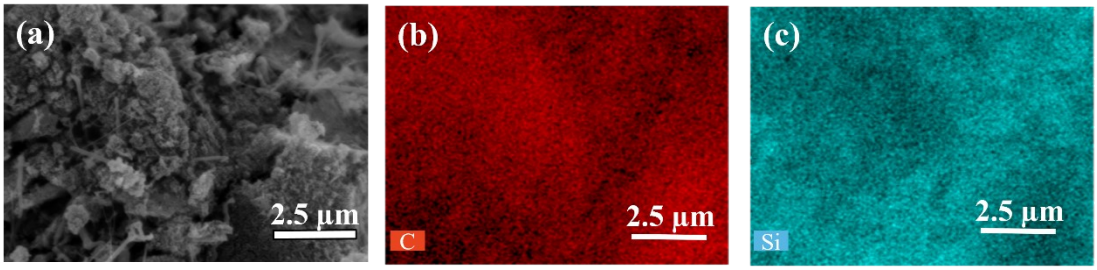

Fig. S7. (a) SEM image of electrode material: EDS of (b) carbon element and (c) silicon element for electrode material.

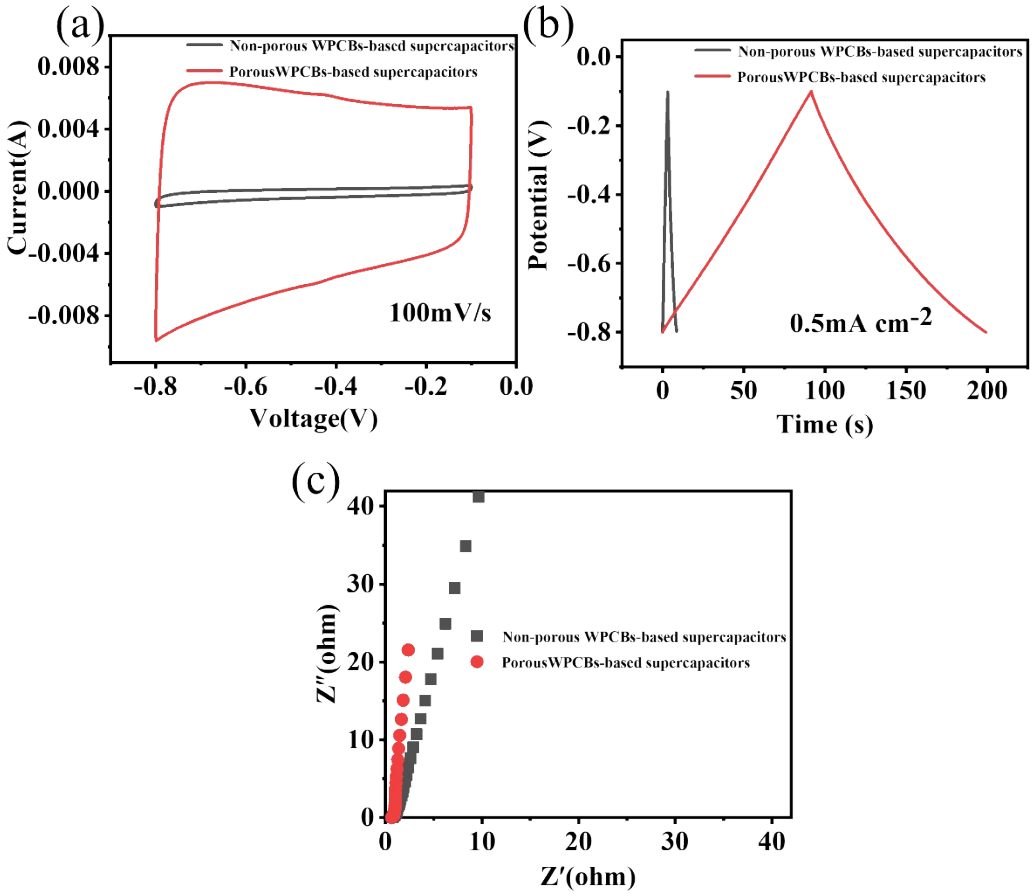

Fig. S8. (a) The CV curves of the non-porous WPCBs-based supercapacitors and the porous

WPCBs-based supercapacitors at scan rate of 100 $mV \cdot s^{-1}$; (b) The GCD curves of the non-porous WPCBs-based supercapacitors and the porous WPCBs-based supercapacitors at 0.5 $mA \cdot cm^{-2}$; (c) The Nyquist plots of the non-porous WPCBs-based supercapacitors and the porous WPCBs-based supercapacitors.

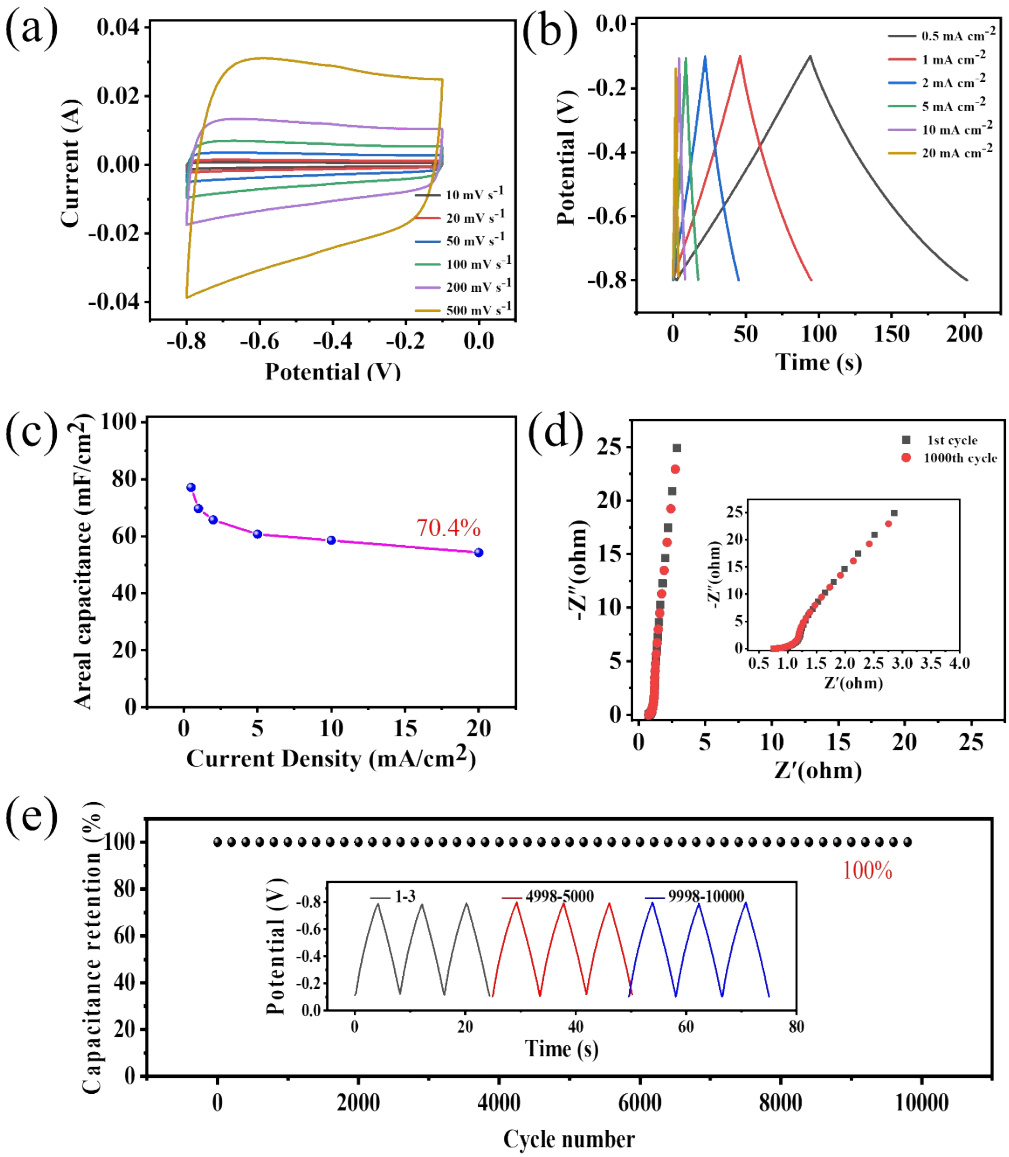

Fig. S9. Electrochemical tests of the porous WPCBs-based supercapacitors at 20 °C with three electrodes: (a) the CV curves of the porous WPCBs-based supercapacitors; (b) the GCD curves of porous WPCBs-based supercapacitors; (c) the capacitance of porous WPCBs-based supercapacitors at various current densities; (d) Nyquist of porous WPCBs-based supercapacitors before and after

10000 cycles; (e) the cycle stability at 10 $mA \cdot cm^{-2}$.